

Fast Surrogate Learning for Multi-Objective UAV Placement in Motorway Intelligent Transportation System

Weian Guo, Shixin Deng, Wuzhao Li, and Li Li

Abstract—We address multi-objective unmanned aerial vehicle (UAV) placement for motorway intelligent transportation systems, where deployments must balance coverage, link quality, and UAV count under geometric constraints. We construct a reproducible benchmark from highD motorway recordings with recording-level splits and generate Pareto-optimal labels via NSGA-II. A preference rule yields deployable targets while preserving multi-objective evaluation. We train fast surrogate models that map unordered vehicle positions to UAV count and continuous placements, using permutation-aware losses and constraint-regularized training across set-based and sequence-based architectures. The evaluation protocol combines Pareto quality metrics, success-rate curves, runtime benchmarks, and robustness studies, with uncertainty quantified by recording-level bootstrap. Results indicate that permutation-invariant set models provide the strongest coverage–SNR–count trade-off among learned predictors and approach NSGA-II quality while enabling real-time inference. Under shared budgets, they offer a more favorable success–latency trade-off than heuristic baselines. The benchmark, splits are released to support reproducible ITS deployment studies and to facilitate comparisons under shared operational budgets.

Index Terms—unmanned aerial vehicles, intelligent transportation systems, UAV placement, multi-objective optimization, surrogate learning, coverage, signal-to-noise ratio.

I. INTRODUCTION

Motorway ITS increasingly relies on timely situational awareness and communication support for tasks such as incident monitoring, temporary congestion handling, vehicle platooning, and closing perception blind spots in complex traffic flows. These tasks are spatially dynamic: density and topology can change within hundreds of meters, and decision latency is constrained by vehicle speeds and safety margins. Fixed roadside units are effective for stable corridors but lack the agility to respond to short-term disruptions or localized coverage gaps. UAVs complement infrastructure by enabling on-demand aerial coverage and flexible network topology adaptation [1], [2].

In a practical traffic management pipeline, UAV placement decisions would be triggered by short-term demand (e.g., queue buildup, incident reports, or V2X relay gaps) and updated on sub-second to minute scales depending on operational

Weian Guo and Shixin Deng are with the Sino-German College of Applied Sciences, Tongji University, Shanghai, China (e-mail: guowei@tongji.edu.cn). Li Li (Corresponding author) is with the School of Electronics and Information Engineering, Tongji University, Shanghai, China (e-mail: lili@tongji.edu.cn). Wuzhao Li (Corresponding author) is with Wenzhou Polytech University, Zhejiang, China. (e-mail:lwzhao055@wzpt.edu.cn)

constraints. For example, a UAV tasked with providing temporary coverage for a congestion wave may need to reposition within tens of seconds, while the placement decision itself must be computed within a fraction of a second to allow integration with scheduling, routing, and safety checks. These system-level requirements motivate a deployment policy that is both accurate (to avoid coverage gaps) and fast (to enable real-time use).

Deploying UAVs in a motorway environment is not a single-objective placement problem. Operators must trade off coverage, link quality, and the number of UAVs while enforcing airspace and safety constraints. In our setting, a decision is required every 0.6 s (15 frames at 25 Hz in highD), and deployment decisions should remain within a typical ITS control loop (tens to hundreds of milliseconds). This makes high-quality optimization desirable but computationally challenging. Classical evolutionary solvers such as NSGA-II can approximate Pareto fronts, yet their per-scene runtime is often too slow for online use. Heuristic methods are fast but may underperform in critical regimes or fail to expose the full coverage–SNR–cost trade-off that deployment operators need.

This paper investigates whether near-NSGA-II multi-objective placement quality can be achieved with millisecond-scale inference suitable for motorway ITS, and whether this yields a better success–latency trade-off than heuristic baselines under a shared UAV budget. Fig. 1 summarizes the end-to-end chain from traffic scene to deployment decision and evaluation. We formalize the task as a multi-objective discrete-continuous optimization problem with explicit bounds and separation constraints, then learn a surrogate predictor that maps vehicle point sets to both UAV count and positions. The surrogate is trained on NSGA-II-generated labels with a preference rule that reflects operational thresholds, and it incorporates permutation-aware learning to handle unordered vehicle sets.

A key challenge for ITS deployment is ensuring that the learned surrogate respects system constraints and is robust to data shifts across recordings. Real traffic data exhibit heterogeneous vehicle densities and lane usage patterns, which can lead to varying spatial extents and non-uniform cluster structures. As a result, naive sequence models may be brittle to input permutations or overfit to recording-specific statistics. We address these risks with permutation-invariant modeling, preference-aware label selection, and explicit constraint projection at inference time.

Compared with UAV-assisted ITS studies that prioritize

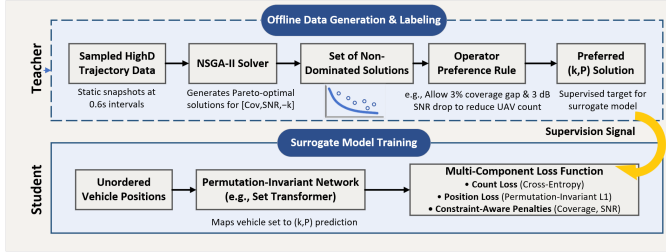


Fig. 1: Problem-to-deployment chain: motorway scenes are mapped to UAV decisions under multi-objective targets and constraints, then evaluated for real-time ITS deployment.

trajectory or resource optimization without real-traffic generalization tests, we focus on static deployment decisions derived from motorway recordings and emphasize recording-level splits to reflect deployment shifts. Compared with learning-to-optimize studies that target fixed output dimensionality or synthetic inputs, we jointly predict the discrete UAV count and continuous placements from unordered vehicle point sets and evaluate multi-objective quality with Pareto metrics and deployment success curves. This framing connects the method to practical ITS decision loops while providing a reproducible benchmark and an evaluation protocol that can be audited by reviewers.

Our main model is a permutation-invariant Set Transformer, complemented by a sequence Transformer and other baselines to characterize inductive biases for unordered traffic scenes. We augment training with constraint-aware losses for coverage and SNR, and apply post-processing to enforce safety constraints. Evaluation follows recording-level splits to avoid leakage across traffic recordings and reports bootstrap confidence intervals, Pareto quality metrics, success-rate curves, and runtime benchmarks on both GPU and CPU. We further analyze robustness to sensor noise, scenario subgroups, and failure modes, and we provide deployment guidelines that link model choice to traffic conditions and latency constraints. The main contributions are:

- **ITS-focused multi-objective benchmark:** a reproducible highD-derived dataset with recording-level splits, explicit constraints, and NSGA-II labels to evaluate UAV deployment under realistic motorway traffic.
- **Preference-guided surrogate learning:** a permutation-aware surrogate framework that predicts both UAV count and positions, with constraint-aware losses and post-processing for safe deployment.
- **Theoretical characterization:** properties of permutation-invariant matching, smooth objective surrogates, and exact-penalty feasibility that justify stable deployment-oriented training.
- **Deployment-oriented evaluation:** a multi-objective, statistically grounded protocol with success-rate curves, Pareto metrics, runtime benchmarks, and robustness analyses that expose system-level trade-offs; under a shared budget, the set-based surrogate achieves higher joint success than greedy/k-means.

The rest of the paper is organized as follows. Section II

reviews related work. Section III formalizes the placement problem and system assumptions. Section IV presents the algorithm design and learning framework. Section V reports the dataset and experimental setup along with results, ablations, and discussion. Section VI concludes the paper.

II. RELATED WORK

A. UAV-Enabled ITS and Air-Ground Deployment

UAV-assisted coverage has been studied in wireless communications and vehicular networks, where aerial base stations can fill coverage gaps or augment roadside infrastructure. Foundational studies analyze air-to-ground path loss and coverage geometry, including altitude selection for maximizing coverage [3] and early UAV small-cell deployment analysis [4]. Surveys and system studies summarize opportunities and challenges of UAV communications in dynamic environments [1]. Recent ITS-focused works address UAV-assisted content delivery, V2X caching, and platoon-aware scheduling, often coupling trajectory planning with resource management [5]–[7]. Additional T-ITS studies explore UAV-assisted RSUs and IoV services under practical constraints [8]–[10]. Complementary T-ITS work studies UAV-enabled data collection and wireless-powered two-way communication services, as well as RIS-UAV relaying for throughput enhancement [11]–[13]. Recent T-ITS studies also investigate URLLC-aware proactive placement, traffic offloading in air-ground integrated networks, and weighted coverage deployment in UAV-enabled sensor systems [14]–[16].

In the ITS context, deployment decisions must also align with transportation constraints such as lane-level coverage, incident response zones, and coordinated V2X scheduling. These system-level considerations motivate the use of real traffic data and evaluation protocols that respect cross-recording generalization, which are often absent in wireless-centric deployment studies. Security and authentication layers are also relevant to UAV-assisted vehicular systems [17], [18], but are typically studied independently of placement decisions. TTV studies further cover QoE/cost-aware resource management, anti-jamming positioning, V2V-assisted 3D deployment, platooning control under uncertain links, blockchain-based edge delivery, temporary UAV-assisted VEC, and network-level modeling or interference-aware trajectory planning [19]–[26].

B. Multi-Objective UAV Placement and Evolutionary Optimization

Multi-objective formulations are common when coverage, SNR, energy, and UAV count must be jointly considered. NSGA-II remains a standard tool for Pareto front approximation [27], and recent wireless optimization studies extend multi-objective formulations to UAV deployment with energy and QoS constraints [28]. In vehicular networks, UAV trajectory and resource management is often optimized for mmWave links, beam tracking, or spectrum sharing [29]–[31]. Joint trajectory and radio resource optimization is also common in TTV studies [32], [33], reflecting the coupling between mobility and link quality. While these approaches can yield

high-quality solutions, they require iterative optimization per scene, making them less suitable for low-latency ITS decision loops.

From a deployment perspective, multi-objective methods are valuable because they expose trade-offs that can be aligned with operator preferences (e.g., fewer UAVs vs. higher SNR). However, without a fast inference surrogate, these trade-offs cannot be exploited in online settings where hundreds of scenes may need to be evaluated per minute.

C. Learning to Optimize on Unordered Inputs

Learning-to-optimize replaces an expensive solver with a fast predictor trained on optimal or near-optimal labels [34]. For unordered spatial inputs, permutation-invariant architectures such as DeepSets [35] and Set Transformers [36] provide principled aggregation, while point-specific attention models [37] and generic attention architectures [38], [39] offer richer interactions. We follow this line in a traffic context: we learn a surrogate that predicts both the number and locations of UAVs from vehicle point sets, and we assess whether such surrogates can preserve Pareto quality and meet ITS runtime requirements.

Unlike many learning-to-optimize setups that assume fixed output dimensionality, UAV placement requires predicting both a discrete count and a set of continuous positions. This creates a permutation ambiguity in the regression target, motivating permutation-invariant losses or matching strategies. We address this ambiguity while maintaining the ability to evaluate multi-objective quality against an NSGA-II reference.

Overall, existing UAV deployment studies seldom evaluate on real traffic data with recording-level splits, and they rarely quantify multi-objective trade-offs using Pareto quality metrics or success-rate curves. Our work aims to close these gaps by combining real motorway data, preference-guided labeling, permutation-aware learning, and deployment-oriented evaluation that explicitly exposes count bias and runtime suitability.

Table I contrasts representative ITS/UAV studies with our placement setting. Most prior works emphasize trajectory/resource control or link-layer objectives, whereas we focus on instantaneous placement with count prediction, Pareto-quality evaluation, and real-traffic generalization. This positioning motivates our emphasis on recording-level splits, budgeted deployment policies, and runtime-aware evaluation.

III. PROBLEM FORMULATION

Consider a motorway scene with a set of vehicles $V = \{v_i \in \mathbb{R}^2\}_{i=1}^N$ in the ground plane. The task is to place k UAVs with horizontal positions $P = \{p_j \in \mathbb{R}^2\}_{j=1}^k$, where $1 \leq k \leq K$ and $K = 3$ in this work. Each UAV operates at a fixed altitude h and must lie within scene bounds $(x_{\min}, x_{\max}, y_{\min}, y_{\max})$. A minimum separation constraint between active UAVs is enforced during post-processing to avoid degenerate colocations. The upper bound $K = 3$ reflects a practical cap on simultaneous UAVs for a single motorway segment given coordination and cost constraints.

A. System Model and Deployment Assumptions

Each scenario is a bounded motorway segment derived from highD. The segment length is 403 m on average (median 414 m), and its width is 31 m (median 31.5 m), covering multi-lane traffic with consistent longitudinal flow. We assume a fixed UAV altitude of 120 m, which aligns with typical low-altitude operational constraints and simplifies coordination with regulatory height limits. The communication model corresponds to downlink broadcast from UAVs to vehicles; coverage radius R represents a service footprint for a target SNR threshold, while mean SNR captures link quality for continuous monitoring or V2X relay. The spatial bounds and minimum separation constraints correspond to geo-fencing and collision-avoidance requirements; they also limit co-channel interference by avoiding colocated aerial relays.

We interpret SNR thresholds as operator-defined service tiers in the robustness analysis: 43 dB for low-rate broadcast/monitoring, 45 dB for standard V2X messaging, and 47 dB for high-reliability demands. Table II provides an illustrative mapping to target BLERs and representative MCS/throughput classes for a 10 MHz channel. This mapping is intended for interpretability and should be replaced by link-level MCS-versus-SNR curves of the target PHY; operators can then adjust policies by increasing P_{tx} , increasing the budgeted UAV count, or relaxing the threshold under adverse propagation.

Unless otherwise noted, we use the parameter values in Table III, including $h = 120$ m, $R = 80$ m, $P_{\text{tx}} = 30$ dBm, $N_0 = -95$ dBm (10 MHz bandwidth, 9 dB noise figure), and $\eta = 2.2$.

B. Coverage

Let R be the communication radius. A vehicle v_i is covered if its horizontal distance to at least one UAV is within R :

$$\mathcal{C}(v_i, P) = \mathbb{I} \left(\min_{j \in \{1, \dots, k\}} \|v_i - p_j\|_2 \leq R \right). \quad (1)$$

The coverage ratio is

$$\text{Cov}(V, P) = \frac{1}{N} \sum_{i=1}^N \mathcal{C}(v_i, P). \quad (2)$$

C. Signal-to-Noise Ratio

For each vehicle, the 3D distance to UAV j is $d_{ij} = \sqrt{\|v_i - p_j\|_2^2 + h^2}$. With a path-loss model

$$L(d_{ij}) = L_0 + 10\eta \log_{10}(d_{ij}), \quad (3)$$

the received SNR in dB from the best UAV is

$$\text{SNR}_i = P_{\text{tx}} - L(d_{i*}) - N_0, \quad (4)$$

where $d_{i*} = \min_j d_{ij}$, P_{tx} is transmit power, and N_0 is the noise floor. We set $L_0 = 32.4$ dB at 1 m and $N_0 = -95$ dBm, corresponding to a 10 MHz bandwidth with a 9 dB noise figure (Table III). The mean SNR is

$$\text{SNR}(V, P) = \frac{1}{N} \sum_{i=1}^N \text{SNR}_i. \quad (5)$$

TABLE I: Representative ITS/UAV studies and their primary focus relative to our placement setting.

Work	Primary focus (from title/abstract)	Relation to our setting
Al-Hilo [5]	Joint UAV trajectory planning and cache management for ITS content delivery	We focus on static placement from traffic snapshots with multi-objective coverage/SNR/count; caching and trajectory planning are not modeled.
Liu [7]	UAV-assisted MEC scheduling for platooning vehicles	Our setting replaces MEC scheduling with placement and emphasizes Pareto quality and deployment latency.
Andreou [8]	Voronoi-based UAV-assisted RSU placement	We learn placement from real trajectories and evaluate multi-objective trade-offs and runtime, beyond geometric placement rules.
Liu [9]	Joint communication and trajectory optimization for multi-UAV IoV	Our work targets instantaneous placement with count prediction instead of trajectory optimization.
Jang [30]	Beam tracking for vehicular communications via UAV-assisted cellular networks	Physical-layer beam tracking is central, whereas placement and count prediction are central in our study.
Spampinato [32]	Joint trajectory design and radio resource management	We isolate placement with multi-objective evaluation and real-traffic generalization rather than trajectory/resource co-optimization.

TABLE II: Illustrative service-tier mapping for SNR thresholds (10 MHz channel).

Tier (SNR)	Service	BLER target	MCS	Spec. eff. (b/s/Hz)
T1 (43 dB)	Broadcast/monitor	$\leq 10^{-2}$	QPSK 1/2	~ 1 b/s/Hz
T2 (45 dB)	Standard V2X	$\leq 10^{-3}$	16QAM 1/2	~ 2 b/s/Hz
T3 (47 dB)	High rel.	$\leq 10^{-5}$	64QAM 1/2	~ 3 b/s/Hz

TABLE III: System parameters with physical meaning and sources.

Parameter	Value	Meaning / source
UAV altitude h	120 m	Fixed low-altitude deployment
Coverage radius R	80 m	Service footprint for target SNR
Transmit power P_{tx}	30 dBm	Typical UAV TX budget
Noise floor N_0	-95 dBm	10 MHz, 9 dB NF
Path-loss exponent η	2.2	Near-LoS urban macro
Reference loss L_0	32.4 dB (@1 m)	Free-space baseline
Min UAV separation	15 m	Collision/safety buffer

We assume a noise-limited channel and do not model interference or shadowing; this corresponds to an orthogonal resource allocation across UAVs (e.g., time/frequency scheduling) and represents a best-case link model.

D. Multi-Objective Formulation

We seek UAV positions that maximize coverage and mean SNR while minimizing the number of UAVs:

$$\max_{P, k} [\text{Cov}(V, P), \text{SNR}(V, P), -k], \quad (6)$$

subject to $1 \leq k \leq K$, p_j within bounds, and a minimum separation constraint between active UAVs:

$$\|p_a - p_b\|_2 \geq d_{\min}, \quad \forall a \neq b. \quad (7)$$

The optimization is multi-objective and non-convex; we use NSGA-II to approximate Pareto-optimal solutions and select training labels. The preference thresholds used to select labels are treated as operator policy parameters; alternative policies can be accommodated by re-labeling or by conditioning the surrogate on desired thresholds.

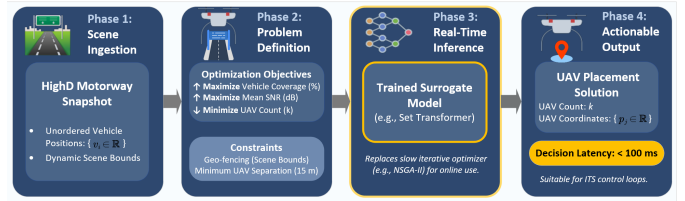


Fig. 2: End-to-end pipeline: highD scenarios are labeled by NSGA-II and used to train surrogate predictors for UAV count and placement.

IV. ALGORITHM DESIGN AND LEARNING FRAMEWORK

We propose a surrogate mapping from unordered vehicle positions to a joint decision: the UAV count class (1–3) and up to three UAV positions in the horizontal plane. The algorithmic contribution is a unified design that (i) predicts discrete counts and continuous placements from sets, (ii) removes label-order ambiguity through permutation-invariant matching, and (iii) aligns training with operational constraints via coverage/SNR surrogates and feasibility projection. Together, these components replace iterative multi-objective search with millisecond-scale inference while preserving deployable placements.

A. Surrogate Architecture

Our main model is a Set Transformer [36], which is permutation-invariant by design and thus aligned with unordered vehicle inputs. Each vehicle (x, y) is embedded into a $d = 128$ token, then processed by two Induced Set Attention Blocks (ISAB) with 16 inducing points to capture long-range interactions at moderate complexity. A pooled multihead attention (PMA) module aggregates the set into a global scene representation. Two heads then predict the UAV count and UAV positions. This design preserves order invariance while allowing global context aggregation, which is useful for long motorway corridors with variable density.

Algorithm 1 Deployment inference with constraint projection

- 1: Input vehicle set V , bounds $(x_{\min}, x_{\max}, y_{\min}, y_{\max})$.
- 2: Predict count \hat{k} and positions \hat{P} with surrogate model.
- 3: Mask inactive UAV slots based on \hat{k} .
- 4: Project \hat{P} to satisfy bounds and minimum separation.
- 5: Output feasible UAV placements P^* .

B. Permutation-Invariant Matching and Constraint-Aware Loss

Because the UAV label set has no canonical ordering, we minimize a permutation-invariant L_1 loss that matches predicted UAV positions to the closest permutation of the ground-truth set, avoiding order ambiguity when $k > 1$. We combine this with a cross-entropy loss for count classification so that the surrogate jointly predicts discrete and continuous decision variables. To align training with operational objectives, we augment the loss with smooth coverage and SNR surrogates and a separation penalty, nudging the model toward feasible placements without explicit iterative optimization.

C. Post-Processing and Constraint Enforcement

At inference, predicted UAV positions are optionally projected to satisfy scene bounds and a minimum separation constraint. The projection iteratively pushes UAV pairs apart when their distance is below 15 m and clamps positions to the scene bounds. We also evaluate a coverage-aware repair step that repositions UAVs toward uncovered vehicles while preserving separation, enabling a trade-off between constraint satisfaction and coverage. These steps emulate practical deployment policies where collision avoidance and geo-fencing are mandatory, and they provide explicit control over feasibility vs. performance.

D. Training Protocol

We split recordings into train/validation/test sets with a 60/20/20 ratio to avoid scene leakage. We create three independent split seeds (2025, 2026, 2027) and use the 2025 split for the main results reported here. Min-max scalers are fitted on the training split only and reused for validation and test data. All runs fix random seeds for NumPy and PyTorch. For sequence-based models, we apply random permutation augmentation of vehicle order during training to reduce ordering bias.

Each model jointly predicts UAV count and positions, aligning the surrogate with the decision variables in the optimization formulation. We use a cross-entropy loss for count classification and a permutation-invariant L_1 loss for positions that matches the predicted UAV set to the closest permutation of the ground-truth set. A weighted sum of count and position losses is optimized using Adam with early stopping (patience 20). Models are trained with a batch size of 64 and learning rate 10^{-3} unless otherwise noted by the architecture defaults.

We augment the training objective with constraint-aware penalties computed from predicted UAV locations and vehicle positions. Coverage is encouraged via a smooth coverage probability with sigmoid temperature $\tau = 5$, SNR is encouraged

via a softmin assignment with temperature $\tau = 20$, and diversity can be enforced by penalizing UAV pairs closer than 15 m. We use a coverage target of 0.97 and minimum SNR of 45 dB (Table III), with loss weights 5.0 (coverage) and 0.5 (SNR) for the main model. The diversity penalty is evaluated as an ablation.

E. Theoretical Properties

We summarize theoretical properties that justify the learning formulation and its alignment with the discrete deployment objectives. Let $d_{ij} = \|v_i - p_j\|_2$ denote horizontal distances, $\sigma(\cdot)$ be the logistic sigmoid, and define the smooth coverage and softmin distances used in training:

$$\begin{aligned} \tilde{c}_i &= \max_j \sigma\left(\frac{R - d_{ij}}{\tau}\right), \\ \bar{d}_i &= \sum_j w_{ij} d_{ij}, \quad w_{ij} = \frac{\exp(-d_{ij}/\tau)}{\sum_\ell \exp(-d_{i\ell}/\tau)}. \end{aligned} \quad (8)$$

The mean soft coverage is $\tilde{\text{Cov}} = \frac{1}{N} \sum_i \tilde{c}_i$ and the soft SNR is computed from \bar{d}_i as in Section III.

a) Proposition 1 (Permutation-invariant matching).

Let $\mathcal{L}_{\text{match}}(P, G) = \min_{\pi \in S_k} \sum_{j=1}^k \|p_j - g_{\pi(j)}\|_1$. Then $\mathcal{L}_{\text{match}}(P, G)$ is invariant to any permutation of G (or P), and $\mathcal{L}_{\text{match}}(P, G) = 0$ iff the two sets are identical up to permutation. *Proof.* For any permutation σ , the feasible set $\{\pi \circ \sigma : \pi \in S_k\}$ equals S_k , so the minimum assignment cost is unchanged. If P and G match up to permutation, one permutation yields zero cost, and conversely zero cost implies elementwise equality under some permutation. \square

b) Proposition 2 (Consistency of smooth coverage). For each vehicle i , $\tilde{c}_i \rightarrow \mathbb{I}(\min_j d_{ij} \leq R)$ pointwise as $\tau \rightarrow 0$, and therefore $\tilde{\text{Cov}} \rightarrow \text{Cov}$. *Proof.* Since $\sigma((R - d)/\tau)$ converges to the step function at $d = R$ as $\tau \rightarrow 0$, the maximum over j converges to the indicator that at least one UAV lies within radius R . Averaging preserves convergence. \square

c) Proposition 3 (Softmin concentration). The softmin weights w_{ij} concentrate on the nearest UAV as $\tau \rightarrow 0$, and $\bar{d}_i \rightarrow \min_j d_{ij}$. *Proof.* For $\tau \rightarrow 0$, the softmax over $-d_{ij}/\tau$ concentrates on the smallest distance index, yielding a one-hot distribution and thus \bar{d}_i equal to the minimum distance. \square

d) Proposition 4 (Exact-penalty feasibility). Define the penalized loss

$$\begin{aligned} \mathcal{L} &= \mathcal{L}_{\text{match}} + \lambda_k \mathcal{L}_{\text{count}} \\ &\quad + \lambda_c [C^* - \tilde{\text{Cov}}]_+ \\ &\quad + \lambda_s [S^* - \tilde{\text{SNR}}]_+ \\ &\quad + \lambda_d \sum_{a < b} [d_{\min} - \|p_a - p_b\|]_+^2. \end{aligned} \quad (9)$$

All penalty terms are nonnegative and vanish iff the corresponding constraint is satisfied. Hence any feasible solution is a minimizer of the penalty terms, and increasing $(\lambda_c, \lambda_s, \lambda_d)$ drives minimizers toward the feasible set whenever it is nonempty. *Proof.* Each hinge term is zero exactly when its constraint holds and positive otherwise, so feasible points incur no penalty. The standard exact-penalty argument applies by taking penalty weights sufficiently large. \square

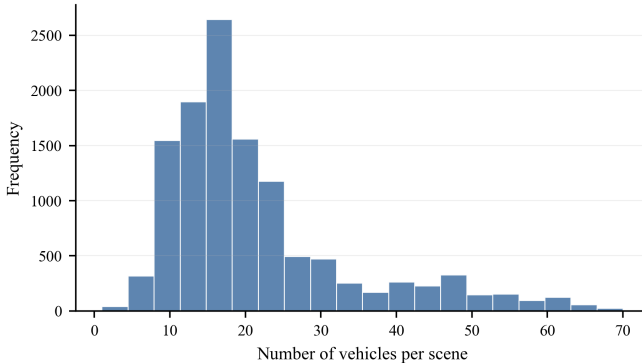


Fig. 3: Distribution of vehicle counts per scene.

e) *Proposition 5 (Lipschitz stability).*: Let P and P' be two UAV sets with $\delta = \max_j \|p_j - p'_j\|_2$. Then $|\tilde{c}_i(P) - \tilde{c}_i(P')| \leq \delta/(4\tau)$ and $|\tilde{\text{Cov}}(P) - \text{Cov}(P')| \leq \delta/(4\tau)$. Moreover, $|\bar{d}_i(P) - \bar{d}_i(P')| \leq \delta$, and the induced soft SNR satisfies $|\tilde{\text{SNR}}(P) - \tilde{\text{SNR}}(P')| \leq L_s \delta$ for some constant L_s depending on the path-loss parameters. *Proof.* σ is $1/4$ -Lipschitz, so $\sigma((R - d)/\tau)$ is $(4\tau)^{-1}$ -Lipschitz in d . The max and average preserve Lipschitz constants, and d_{ij} is 1 -Lipschitz in p_j . For \bar{d}_i , all d_{ij} shift by at most δ , so the min and max shift by at most δ , and \bar{d}_i lies between them. The SNR mapping is smooth on bounded distances, yielding a finite L_s . \square

V. EXPERIMENTS, RESULTS, AND DISCUSSION

A. Dataset and Labeling

1) *Dataset and Label Generation*: We build a supervised dataset from the highD motorway recordings [40], captured by drones at 25 Hz over German highways with multiple lanes and unobstructed top-down views. We use 20 recordings (out of the full highD set) and sample frames every 15 time steps (0.6 s) up to 300 frames per recording to create static snapshots of vehicle positions. For each frame, we compute scene bounds from vehicle extents and add a small margin to allow UAV placement beyond the convex hull of vehicles. Vehicles within each frame are ordered by track ID (as provided by highD) to obtain a deterministic sequence for order-sensitive models; this ordering is randomized during training to mitigate permutation sensitivity (Section IV-D).

a) *Dataset statistics*: The integrated dataset contains 12,000 scenarios spanning 20 recordings. Each sample includes up to 70 vehicle positions (mean 21.44, median 18, 95th percentile 50), a UAV count label in $\{1, 2, 3\}$, and up to three UAV positions. The distribution of vehicle counts is shown in Fig. 3. Per-recording vehicle counts range from 12.3 to 54.7 on average, reflecting diverse traffic densities. Recording-level splits are used to prevent leakage across training and test scenes; the split protocol is summarized in Section V-B. Because frames within the same recording are temporally correlated, we report bootstrap confidence intervals at the recording level and include a sparser sampling ablation (30-frame stride) to validate robustness.

TABLE IV: Recording-level vehicle count statistics.

Recording ID	Samples	Mean vehicles	Median vehicles	Max vehicles
1	600	16.70	17	29
2	600	14.50	14	32
3	600	12.27	12	24
4	600	14.76	15	25
5	600	13.87	14	23
6	600	16.17	16	25
7	600	17.70	17	32
8	600	16.84	16	31
9	600	15.21	15	26
10	600	18.63	19	37
11	600	44.56	44	62
12	600	54.68	56	70
13	600	39.34	40	57
15	600	17.14	17	35
16	600	14.34	15	29
18	600	13.71	14	24
22	600	17.39	17	34
23	600	18.56	19	32
40	600	28.45	28	42
58	600	23.97	23	40

Algorithm 2 Label generation and surrogate training

- 1: Sample frames from each recording and build vehicle sets V .
- 2: **for** each scenario **do**
- 3: Run NSGA-II to obtain a Pareto front.
- 4: Select a preferred solution under coverage/SNR tolerances.
- 5: Store UAV count and positions as labels.
- 6: **end for**
- 7: Train a surrogate predictor on $\{(V, \text{labels})\}$.

b) *Recording statistics*: Table IV reports per-recording vehicle counts for the 20 highD recordings used in this study (600 sampled frames per recording).

c) *NSGA-II label generation*: For each scenario, NSGA-II [27] optimizes three objectives: coverage gap ($1 - \text{Cov}$), UAV count k , and negative mean SNR ($-\text{SNR}$). We use a population size of 32, 60 generations, and allow $k \in [1, 3]$. After obtaining the Pareto front, a preference rule selects a single label by (i) allowing a 3% coverage gap from the best solution, (ii) allowing a 3 dB drop in mean SNR within that subset, and (iii) preferring fewer UAVs. These thresholds align with our deployment targets of 97% coverage and 45 dB mean SNR (Table III) and reflect a typical operator policy: allow small quality drops to reduce the number of UAVs when the coverage/SNR difference is marginal. A sensitivity study over (1%, 2%, 3%, 5%) coverage tolerances and (1, 2, 3, 5) dB SNR tolerances shows that the selected k distribution and mean objectives vary only slightly, indicating that the dataset is not overly sensitive to small preference changes. NSGA-II uses crossover rate 0.9, mutation rate 0.2, and a position mutation standard deviation of 15 m. NSGA-II labeling cost averages 0.41 s per scenario on our CPU (5 samples: 2.09 s), yielding a total labeling time of roughly 1.4 hours for 12,000 scenarios; this process is embarrassingly parallel.

UAV positions in the dataset are stored in fixed slots, but the label set has no canonical ordering. We therefore treat the labels as unordered and use permutation-invariant matching losses during training to eliminate label-order ambiguity.

TABLE V: Preference sensitivity summary (NSGA-II labels).

Tolerance (Cov., SNR)	Mean k	Coverage	Mean SNR (dB)
1%, 1 dB	2.65	0.9987	46.398
5%, 5 dB	2.63	0.9975	46.390

d) Preference sensitivity.: Across coverage tolerances $\{1\%, 2\%, 3\%, 5\%\}$ and SNR tolerances $\{1, 2, 3, 5\}$ dB, the selected label distribution remains stable with mean k between 2.62 and 2.65. Mean coverage stays within $[0.9975, 0.9987]$ and mean SNR within $[46.39, 46.40]$ dB, indicating mild sensitivity to preference thresholds.

B. Experimental Setup

1) Dataset and Splits: We use the highD-derived dataset described in Section V-A1, containing 12,000 scenarios across 20 recordings. Recording-level splits are used to avoid scene leakage, with a 60/20/20 train/validation/test ratio. We create three independent splits (seeds 2025, 2026, 2027); the main paper reports the 2025 split with bootstrap confidence intervals, and additional split results are provided in the released code. Frames are sampled every 15 time steps (up to 300 per recording); a 30-frame stride ablation confirms that the main trends are robust to sparser sampling.

2) Models, Baselines, and Training: We compare against a greedy coverage heuristic, a k-means placement heuristic, and an oracle using the NSGA-II label solution. The learned models include a Transformer, a 1D CNN with Transformer head, a U-Net on occupancy grids, DeepSets, and a Set Transformer baseline.

All models are trained with Adam (learning rate 10^{-3} , batch size 64) and early stopping on the validation split. The Transformer uses a 3-layer encoder with 8 heads; the 1D CNN uses residual blocks with attention and a 3-layer Transformer head; the U-Net operates on 128×128 occupancy grids; and DeepSets uses mean/max pooling. K-means uses 20 iterations, and the greedy baseline selects UAVs by incremental coverage gain. For post-processing, we apply 10 projection iterations and a minimum separation of 15 m. Each reported model is trained once per split with the same data and optimization budget.

3) Metrics and Evaluation Protocol: We report UAV count accuracy, mean coverage ratio, and mean SNR on the test recordings. Confidence intervals are computed with 500 bootstrap resamples over recordings. We additionally report success rates for coverage ≥ 0.95 and mean SNR ≥ 45 dB, and track the predicted count distribution to quantify over/under-deployment. To expose operational trade-offs, we evaluate success-rate curves over coverage and SNR thresholds (Section V-C). Predicted UAV positions are optionally post-processed to enforce bounds and a minimum separation of 15 m.

For multi-objective quality, we compute generational distance (GD), inverted generational distance (IGD), and dominated hypervolume (HV) in a normalized objective space. Pareto fronts are approximated with NSGA-II for a subset of 100 test scenarios. Objectives are normalized by coverage

gap in $[0, 1]$, UAV count divided by $k_{\text{ref}} = 4$, and negative SNR divided by 120, with a reference point at $(1, 1, 1)$. We further report paired Wilcoxon tests for GD/IGD/HV against the Transformer baseline.

All learned models receive the same vehicle positions as inputs and are evaluated with identical normalization and post-processing policies. Models are evaluated under two masking policies: using the ground-truth count (mask-by true) and using the predicted count (mask-by pred). For heuristics, we use the ground-truth UAV count since these methods do not predict k . Hyperparameters for all baselines are fixed across splits; no per-recording tuning is performed. We report recording-level bootstrap confidence intervals to account for within-recording temporal correlation.

4) Hardware, Software, and Runtime Protocol: All experiments are run on a Windows 11 workstation with an Intel Core i7-13790F CPU (24 logical processors) and an NVIDIA RTX 4090 GPU. The software stack includes Python 3.12.7, PyTorch 2.7.1, NumPy 1.26.4, and Pandas 2.2.2.

Inference runtime is measured on 200 test samples for GPU and 50 test samples for CPU, while NSGA-II timing is measured on 10 (GPU) or 5 (CPU) samples due to its cost. We report end-to-end latency (including preprocessing and post-processing) for batch sizes 1 and 64 on GPU, and batch size 1 on CPU, plus throughput in samples per second. Section V-C summarizes the batch size 1 results.

C. Results and Analysis

Table VI reports cross-recording results on the seed-2025 split under the budget-matched count policy (Policy B, mean $k = 2.74$). The Set Transformer achieves the strongest coverage–SNR trade-off among learned models and yields the highest joint success rate at the shared budget (0.791). Greedy and k-means remain competitive on coverage and SNR but are consistently lower in joint success, while the facility-location baseline (k-medoids) trails k-means/greedy under the shared budget. The Transformer benefits from constraint-aware training but remains less accurate in count prediction (0.747 vs. 0.950 for the Set Transformer). Bootstrap confidence intervals are computed over four test recordings.

Across bootstrap resamples, the confidence intervals remain narrow for coverage and SNR, indicating stable generalization. Coverage shows modest variance for the Transformer but remains consistently above the CNN and DeepSets baselines. Using success thresholds of coverage ≥ 0.95 and SNR ≥ 45 dB, the Set Transformer achieves a success rate of 0.791, outperforming greedy (0.644), k-means (0.760), and k-medoids (0.588), while remaining below the oracle upper bound (0.881).

Fig. 4 summarizes the success–latency trade-off under Policy B. The Set Transformer dominates greedy, k-means, and k-medoids by achieving higher joint success at substantially lower latency, while the oracle upper bound remains far slower.

Table IX reports Pareto quality metrics computed on 100 sampled test scenarios (mask-by true). Lower GD/IGD and higher HV indicate closer alignment to the NSGA-II front. Set Transformer attains the lowest GD among learned models, while the Transformer achieves competitive HV; paired

TABLE VI: Cross-recording results under Policy B (budget-matched k , mean $k = 2.74$). Success uses $\text{Cov} \geq 0.95$ and $\text{SNR} \geq 45$ dB.

Model	Coverage	Mean SNR (dB)	Success rate
Transformer	0.928 [0.901, 0.956]	46.132 [46.044, 46.219]	0.625 [0.521, 0.730]
Set Transformer	0.957 [0.936, 0.977]	46.252 [46.179, 46.325]	0.791 [0.708, 0.873]
1D CNN + Transformer	0.527 [0.524, 0.531]	44.877 [44.862, 44.889]	0.003 [0.000, 0.006]
Picture CNN (U-Net)	0.475 [0.467, 0.483]	44.497 [44.450, 44.533]	0.003 [0.001, 0.006]
DeepSets	0.583 [0.564, 0.597]	45.091 [45.027, 45.152]	0.013 [0.005, 0.021]
Greedy	0.955 [0.942, 0.967]	46.208 [46.175, 46.239]	0.644 [0.573, 0.715]
K-means	0.964 [0.953, 0.975]	46.374 [46.342, 46.405]	0.760 [0.703, 0.819]
K-medoids	0.941 [0.923, 0.959]	46.339 [46.301, 46.373]	0.588 [0.516, 0.683]
<i>Upper bound (not budgeted)</i>			
Oracle (preferred NSGA-II label)	0.967 [0.953, 0.981]	46.293 [46.231, 46.354]	0.881 [0.828, 0.933]

TABLE VII: Runtime benchmark on GPU (batch size 1, end-to-end ms, speedup vs. NSGA-II).

Method	Params (M)	Time (ms)	Speedup
Transformer	4.08	1.20	3785 \times
Set Transformer	0.54	2.44	1870 \times
1D CNN + Transformer	8.32	4.59	993 \times
Picture CNN (U-Net)	6.12	1.95	2342 \times
DeepSets	0.09	0.80	5719 \times
Greedy	—	54.19	84 \times
K-means	—	105.88	43 \times
K-medoids	—	18.18	251 \times
NSGA-II	—	4556.1	1 \times

TABLE VIII: Deployment success vs. latency under Policy B (success: $\text{Cov} \geq 0.95$ and $\text{SNR} \geq 45$ dB).

Method	Success rate	GPU ms	CPU ms
Set Transformer	0.791	2.44	4.01
Transformer	0.625	1.20	13.45
Greedy	0.644	54.19	64.72
K-means	0.760	105.88	116.45
K-medoids	0.588	18.18	19.68
NSGA-II (oracle)	0.881	4556.1	4565.7

Wilcoxon tests confirm statistically significant differences for most baselines.

Among learned models, Set Transformer attains the lowest GD (0.007) and the highest HV (0.436), indicating closer alignment to the NSGA-II front. DeepSets exhibits lower IGD but substantially lower HV, suggesting that its solutions are less competitive across the full objective range.

The runtime results highlight a clear trade-off between inference speed and coverage quality. DeepSets is the fastest learned model, while the Transformer and Set Transformer provide a strong balance between accuracy and speed and remain well within typical ITS real-time constraints (e.g., <100 ms per decision). On CPU, batch-1 end-to-end latency is 13.45 ms for the Transformer and 4.01 ms for the Set Transformer, still far below typical control-loop budgets. Table VIII summarizes deployment-level trade-offs using a joint success criterion (coverage ≥ 0.95 and SNR ≥ 45 dB). The Set Transformer yields the highest success rate among learned models while remaining three orders of magnitude faster than

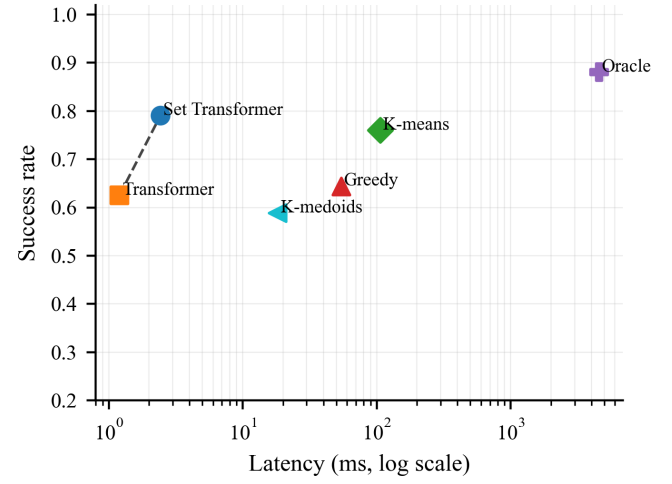


Fig. 4: Success–latency scatter under Policy B (log-scale latency). The dashed line connects non-dominated points.

NSGA-II, whereas the Transformer offers lower success with the lowest GPU latency.

1) *Sensitivity Analyses*: Fig. 5 shows success rates as the coverage and SNR thresholds vary under Policy B. At a fixed SNR threshold of 45 dB, the Set Transformer maintains a success rate of 0.791 at 95% coverage and 0.780 at 98% coverage, while the Transformer achieves 0.625 and 0.577, respectively. K-means remains competitive at moderate thresholds (0.760 at 95% coverage) but degrades more sharply as coverage thresholds increase. Success rates remain flat between 40 and 46 dB and collapse at 47 dB, indicating that the mean SNR distribution concentrates near 46 dB for all methods.

We further evaluate robustness to position noise to reflect localization errors in deployment.

Fig. 6 reports sensitivity to Gaussian GNSS noise in vehicle positions. The Transformer shows negligible change in coverage and success up to 5 m noise (0.825 throughout), and the Set Transformer degrades mildly (success drops from 0.865 to 0.853 at 5 m). Greedy is more sensitive: success falls from 0.668 to 0.551, indicating that learned models are more robust to moderate localization noise. These bounded degradations are consistent with the Lipschitz stability in Proposition 5. The permutation sensitivity results in Section V-D empirically

TABLE IX: Pareto metrics on sampled test scenarios (mean with 95% CI, mask-by true).

Model	GD ↓	IGD ↓	HV ↑
Transformer	0.012 [0.004, 0.025]	0.445 [0.422, 0.465]	0.406 [0.384, 0.431]
Set Transformer	0.007 [0.003, 0.012]	0.462 [0.441, 0.481]	0.436 [0.410, 0.471]
DeepSets	0.046 [0.034, 0.057]	0.379 [0.364, 0.393]	0.292 [0.263, 0.328]
Greedy	0.003 [0.002, 0.006]	0.454 [0.435, 0.472]	0.435 [0.408, 0.471]
K-means	0.005 [0.001, 0.011]	0.469 [0.449, 0.489]	0.447 [0.418, 0.485]
Oracle (NSGA-II label)	0.009 [0.004, 0.015]	0.484 [0.468, 0.501]	0.461 [0.429, 0.502]

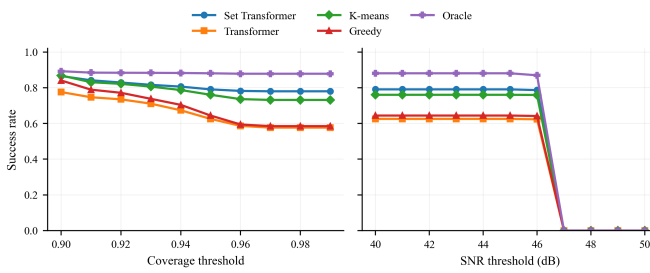
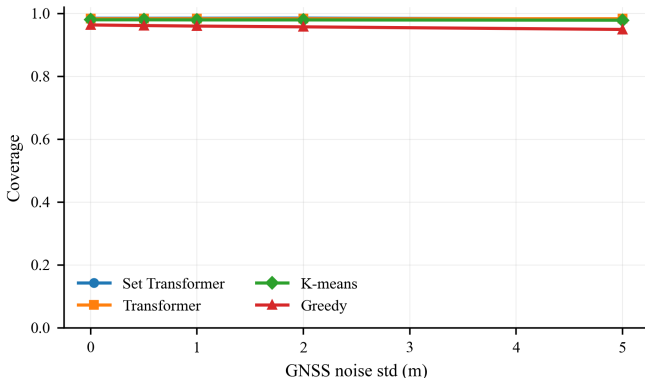
Fig. 5: Success-rate curves versus coverage and SNR thresholds under Policy B (budget-matched k).

Fig. 6: Coverage under GNSS noise (mask-by pred for learned models, mask-by true for heuristics).

support Proposition 1.

2) *Failure Case and Subset Analysis*: Table X summarizes failure rates across density and elongation clusters, where failure is coverage < 0.90 or SNR < 45 dB. Low-density and highly elongated scenes exhibit the highest failure rates (5–6%). High-density scenes with moderate elongation have near-zero failure rates, and Fig. 7 visualizes this trend.

To assess failure modes, we inspect low-coverage Transformer predictions on the test split. A representative case shows vehicles occupying a long, sparse corridor and the predicted UAVs clustering near one region, leaving distant vehicles uncovered. A cluster analysis confirms higher failure rates (5–6%) in low-density, highly elongated scenes, while dense scenes exhibit near-zero failure rates.

Table XI compares joint success across density/elongation clusters under the shared budget (Policy B). The Set Transformer exceeds the best heuristic in 7 of 9 clusters, with the largest gains in elongated scenes (e.g., +0.086 in mid/high

TABLE X: Failure rates by density and elongation cluster (Transformer, mask-by pred).

Cluster	Failure rate	Coverage	Mean SNR (dB)
Low dens., low el.	0.054	0.986	46.320
Low dens., mid el.	0.058	0.981	46.322
Low dens., high el.	0.058	0.979	46.273
Mid dens., low el.	0.017	0.988	46.327
Mid dens., mid el.	0.030	0.985	46.334
Mid dens., high el.	0.034	0.977	46.299
High dens., low el.	0.010	0.984	46.322
High dens., mid el.	0.000	0.987	46.339
High dens., high el.	0.017	0.984	46.322

TABLE XI: Clustered success rates under Policy B (budgeted k). Delta is Set Transformer minus the best heuristic.

Cluster	N	Set Trans.	Greedy	K-means	Delta
Low / Low	294	0.673	0.469	0.605	+0.068
Low / Mid	258	0.465	0.341	0.419	+0.047
Low / High	240	0.417	0.300	0.367	+0.050
Mid / Low	293	0.843	0.799	0.867	-0.024
Mid / Mid	267	0.921	0.727	0.873	+0.049
Mid / High	232	0.897	0.616	0.810	+0.086
High / Low	205	0.888	0.932	0.985	-0.098
High / Mid	267	0.993	0.858	0.970	+0.022
High / High	344	0.965	0.747	0.916	+0.049

and +0.049 in high/high), while k-means remains strongest in compact high-density scenes (high/low). These cases highlight the need for stronger spatial diversity or explicit trajectory coupling when scene extents become highly elongated.

D. Ablation Studies

We report four ablations covering training recipe, masking policy, permutation sensitivity, and post-processing. Table XII compares a baseline Transformer trained with count cross-entropy and L_1 regression against the proposed recipe with permutation-invariant matching, random-order augmentation, and constraint-aware losses. The proposed recipe improves coverage by 0.150 while keeping count accuracy unchanged.

Table XIII compares evaluation with ground-truth UAV counts (mask-by true) versus predicted counts (mask-by pred). The Transformer benefits most from mask-by pred because it overpredicts $k = 3$ (mean 3.00, over-rate 25.3%). This increases coverage but can deviate from the count minimization objective, so we report Pareto metrics under both count sources (Section V-C).

Permutation sensitivity is evaluated by averaging 10 random orderings per test sample. The average per-sample standard deviation across permutations is 1.7×10^{-8} for coverage and 6.9×10^{-6} dB for SNR, indicating near permutation invariance under the proposed training recipe.

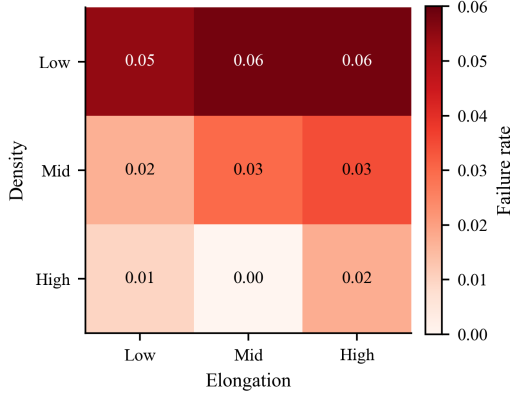


Fig. 7: Failure-rate heatmap by density and elongation (Transformer, mask-by pred).

TABLE XII: Training-recipe ablation for the Transformer (mask-by true, mean with 95% CI).

Model	Count Acc.	Coverage	Mean SNR (dB)
Baseline (CE+ L_1)	0.747 [0.648,0.840]	0.779 [0.762,0.796]	45.872 [45.807,45.944]
Proposed recipe	0.747 [0.648,0.840]	0.929 [0.907,0.950]	46.138 [46.063,46.211]

For post-processing, Table XIV summarizes the Transformer (mask-by pred) before and after projection. Simple projection removes out-of-bounds UAVs without reducing coverage. A coverage-aware repair step further reduces constraint violations at a cost of 2.37 points in coverage. Fig. 8 visualizes the coverage–constraint trade-off across separation thresholds (10/15/20 m).

E. Discussion and Limitations

Our study relies on static snapshots and a simplified air-to-ground channel model. In practice, UAVs must coordinate over time with vehicle motion, energy constraints, and no-fly zones, and propagation is affected by shadowing, interference, and non-line-of-sight conditions. A sensitivity analysis over path-loss exponents $\eta \in \{2.0, 2.2, 2.6, 3.0\}$ shows that coverage remains stable but mean SNR drops from 50.5 dB to 29.5 dB, indicating that deployment performance is highly channel dependent and should be re-optimized when propagation conditions change.

The learned predictors inherit the preference encoded by the NSGA-II label selection (coverage and SNR tolerances). A tolerance sweep yields a stable label distribution (mean k between 2.62 and 2.65), but the Transformer still overpredicts $k = 3$ at inference, which boosts coverage under mask-by pred yet deviates from the count minimization objective. Addressing this bias may require preference-conditioned models, explicit count calibration, or hybrid inference that falls back to heuristics under low confidence. Permutation sensitivity is negligible after random-order augmentation, yet strongly elongated scenes remain failure modes, suggesting a need for stronger diversity constraints or global context.

Scalability beyond $K = 3$ remains a challenge. A $K = 5$ Transformer trained on an expanded 960-scenario subset

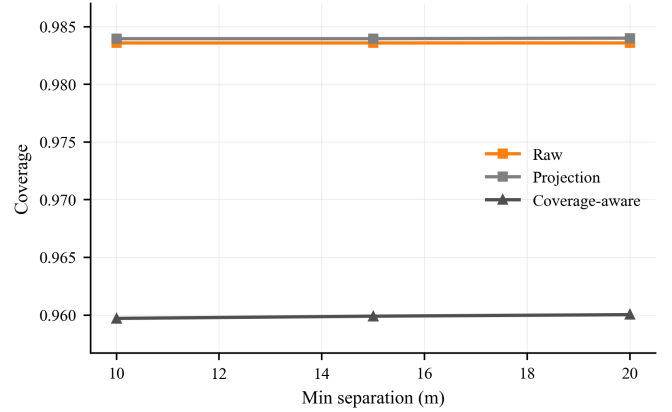


Fig. 8: Post-processing trade-off between coverage and constraint violations at different separation thresholds.

reaches coverage 0.761, mean SNR 45.77 dB, and count accuracy 0.721, still below the $K = 3$ regime, indicating that larger output sets require richer supervision, slot-based assignment, or permutation-invariant matching at higher capacity. This is a key direction for future work.

From a safety and regulatory standpoint, deployments must respect geo-fencing, altitude limits, and separation constraints. Our post-processing provides a lightweight feasibility projection, but practical systems should also handle no-fly zones, dynamic altitude corridors, and explicit collision-avoidance policies. We also find that learned models are robust to moderate GNSS noise (up to 5 m), while greedy heuristics degrade more noticeably; however, larger localization errors or delayed sensing could still lead to unsafe placements. A practical deployment should include uncertainty estimation and fallback policies (e.g., switching to a heuristic or short-horizon optimization when confidence is low), as well as monitoring for failure modes in elongated corridors.

1) *Practical Deployment Guidelines*: Our results suggest the following operational choices. The Set Transformer is preferred when coverage reliability is critical: it maintains the highest success rate across thresholds and is robust to moderate position noise. The Transformer offers a strong accuracy–speed balance and is competitive when compute budgets are tight but coverage thresholds are moderate. DeepSets is suitable for ultra-low latency when coverage is not the dominant objective. In sparse, elongated corridors, heuristic baselines remain strong; a hybrid policy can use heuristics for low-density scenes and learned models for dense or clustered traffic. These guidelines are derived from the success-rate curves, runtime benchmarks, and subset analyses in Section V-C.

To support reproducibility, we will release the code and recording-level splits in a public repository (github.com/highd-uav-its). The highD dataset is publicly available; we will provide the derived labels and train/val/test splits. Future work will incorporate temporal models, more realistic channel models, and additional datasets or real-world measurements to validate deployment robustness.

TABLE XIII: Mask-policy ablation using predicted-count masking (mean with 95% CI).

Model	Coverage	Mean SNR (dB)
Transformer	0.984 [0.982,0.985]	46.318 [46.301,46.330]
Set Transformer	0.985 [0.981,0.989]	46.369 [46.354,46.387]
1D CNN + Transformer	0.527 [0.524,0.530]	44.874 [44.862,44.886]
Picture CNN (U-Net)	0.475 [0.465,0.485]	44.503 [44.446,44.553]
DeepSets	0.585 [0.566,0.600]	45.118 [45.044,45.193]

TABLE XIV: Post-processing ablation for the Transformer (mask-by pred). OOB: out-of-bounds rate.

Setting	Coverage	SNR (dB)	OOB	Sep. viol.
Raw	0.984	46.318	0.0408	0.0000
Projected	0.984	46.327	0.0000	0.0013
Cov.-aware repair	0.960	46.264	0.0042	0.0004

VI. CONCLUSION

We presented a surrogate-learning framework for multi-objective UAV placement in motorway ITS. Using NSGA-II labels from highD recordings, we trained multiple predictors and evaluated them under recording-level splits with confidence intervals and runtime benchmarks. The Set Transformer achieves the highest coverage among learned models, while the Transformer provides a favorable accuracy–speed trade-off. Under a shared budget, the set-based surrogate delivers higher joint success than the heuristic baselines and thus offers a stronger success–latency trade-off for real-time deployment. On the GPU benchmark, learned surrogates operate in the thousand-fold speedup regime over NSGA-II (Table VII), indicating that surrogate placement can meet real-time ITS decision loops under the stated assumptions. The success-rate curves and Pareto metrics further highlight that permutation-invariant modeling yields a more reliable coverage–SNR–count balance, while elongated or low-density scenes remain the dominant failure modes. These findings support a closed-loop deployment view in which placement is refreshed on triggers, projected to satisfy safety constraints, and backed by a fallback heuristic or short local search when confidence is insufficient.

Future work will incorporate temporal dynamics, UAV motion constraints, and energy budgets to move from static snapshots to closed-loop deployment. We also plan to strengthen the propagation model with interference and non-line-of-sight effects and validate the benchmark on additional datasets or field measurements.

REFERENCES

- [1] Y. Zeng, R. Zhang, and T. J. Lim, “Wireless communications with unmanned aerial vehicles: Opportunities and challenges,” *IEEE Communications Magazine*, vol. 54, no. 5, pp. 36–42, 2016.
- [2] M. Mozaffari, W. Saad, M. Bennis, and M. Debbah, “Efficient deployment of multiple unmanned aerial vehicles for optimal wireless coverage,” *IEEE Communications Letters*, vol. 20, no. 8, pp. 1647–1650, 2016.
- [3] A. Al-Hourani, S. Kandeepan, and S. Lardner, “Optimal lap altitude for maximum coverage,” *IEEE Wireless Communications Letters*, vol. 3, no. 6, pp. 569–572, 2014.
- [4] M. Mozaffari, W. Saad, M. Bennis, and M. Debbah, “Drone small cells in the clouds: Design, deployment and performance analysis,” in *2015 IEEE Global Communications Conference (GLOBECOM)*, 2015, pp. 1–6.
- [5] A. Al-Hilo, M. Samir, C. Assi, S. Sharafeddine, and D. Ebrahimi, “Uav-assisted content delivery in intelligent transportation systems-joint trajectory planning and cache management,” *IEEE Transactions on Intelligent Transportation Systems*, vol. 22, no. 8, pp. 5155–5167, 2021.
- [6] R. Zhang, R. Lu, X. Cheng, N. Wang, and L. Yang, “A uav-enabled data dissemination protocol with proactive caching and file sharing in v2x networks,” *IEEE Transactions on Communications*, vol. 69, no. 6, pp. 3930–3942, 2021.
- [7] Y. Liu, J. Zhou, D. Tian, Z. Sheng, X. Duan, G. Qu, and V. Leung, “Joint communication and computation resource scheduling of a uav-assisted mobile edge computing system for platooning vehicles,” *IEEE Transactions on Intelligent Transportation Systems*, vol. 23, no. 7, pp. 8435–8450, 2022.
- [8] A. Andreou, C. X. Mavromoustakis, J. M. Batalla, E. K. Markakis, and G. Mastorakis, “Uav-assisted rsus for v2x connectivity using voronoi diagrams in 6g+ infrastructures,” *IEEE Transactions on Intelligent Transportation Systems*, vol. 24, no. 12, pp. 15 855–15 865, 2023.
- [9] X. Liu, B. Lai, B. Lin, and V. C. M. Leung, “Joint communication and trajectory optimization for multi-uav enabled mobile internet of vehicles,” *IEEE Transactions on Intelligent Transportation Systems*, vol. 23, no. 9, pp. 15 354–15 366, 2022.
- [10] L. Qu, G. Bai, C. Dai, J. Liu, and D. Sun, “Learning-based aoi minimization through uav-assisted data distribution in vehicular networks,” *IEEE Transactions on Intelligent Transportation Systems*, vol. 26, no. 11, pp. 19 645–19 660, 2025.
- [11] X. Li, J. Tan, A. Liu, P. Vijayakumar, N. Kumar, and M. Alazab, “A novel uav-enabled data collection scheme for intelligent transportation system through uav speed control,” *IEEE Transactions on Intelligent Transportation Systems*, vol. 22, no. 4, pp. 2100–2110, 2021.
- [12] G. Park, K. Heo, W. Lee, and K. Lee, “Uav-assisted wireless-powered two-way communications,” *IEEE Transactions on Intelligent Transportation Systems*, vol. 25, no. 3, pp. 2641–2655, 2024.
- [13] X. Liu, Y. Yu, F. Li, and T. S. Durrani, “Throughput maximization for ris-uav relaying communications,” *IEEE Transactions on Intelligent Transportation Systems*, vol. 23, no. 10, pp. 19 569–19 574, 2022.
- [14] C.-F. Liu, N. D. Wickramasinghe, H. A. Suraweera, M. Bennis, and M. Debbah, “Urllc-aware proactive uav placement in internet of vehicles,” *IEEE Transactions on Intelligent Transportation Systems*, vol. 25, no. 8, pp. 10 446–10 451, 2024.
- [15] B. Fan, L. Jiang, Y. Chen, Y. Zhang, and Y. Wu, “Uav assisted traffic offloading in air ground integrated networks with mixed user traffic,” *IEEE Transactions on Intelligent Transportation Systems*, vol. 23, no. 8, pp. 12 601–12 611, 2022.
- [16] X. Zhu and M. Zhou, “Maximal weighted coverage deployment of uav-enabled rechargeable visual sensor networks,” *IEEE Transactions on Intelligent Transportation Systems*, vol. 24, no. 10, pp. 11 293–11 307, 2023.
- [17] J. Miao, Z. Wang, X. Ning, A. Shankar, C. Maple, and J. J. P. C. Rodrigues, “A uav-assisted authentication protocol for internet of vehicles,” *IEEE Transactions on Intelligent Transportation Systems*, vol. 25, no. 8, pp. 10 286–10 297, 2024.
- [18] J. Choi, D. Kwon, and S. Son, “A puf-based lightweight authentication scheme for uav-assisted internet of vehicles,” *IEEE Transactions on Intelligent Transportation Systems*, 2025.
- [19] D. Ferretti, S. Mignardi, R. Marini, R. Verdone, and C. Buratti, “Qoe and cost-aware resource and interference management in aerial-terrestrial networks for vehicular applications,” *IEEE Transactions on Vehicular Technology*, vol. 73, no. 8, pp. 11 249–11 261, 2024.
- [20] Z. Wang, R. Liu, Q. Liu, L. Han, and J. S. Thompson, “Feasibility study of uav-assisted anti-jamming positioning,” *IEEE Transactions on Vehicular Technology*, vol. 70, no. 8, pp. 7718–7733, 2021.
- [21] B. Zhang, Z. He, Y. Feng, and Z. Han, “Performance analysis and 3d position deployment for v2v-assisted uav communications in vehicular networks,” *IEEE Transactions on Vehicular Technology*, vol. 73, no. 12, pp. 19 361–19 373, 2024.

- [22] X. Duan, Y. Zhao, D. Tian, J. Zhou, L. Ma, and L. Zhang, "Joint communication and control optimization of a uav-assisted multi-vehicle platooning system in uncertain communication environment," *IEEE Transactions on Vehicular Technology*, vol. 73, no. 3, pp. 3177–3190, 2024.
- [23] Q. Xu, J. Jin, Z. Su, R. Li, Y. Wang, D. Fang, and Y. Wu, "Blockchain-based layered secure edge content delivery in uav-assisted vehicular networks," *IEEE Transactions on Vehicular Technology*, vol. 74, no. 5, pp. 7914–7927, 2025.
- [24] C. Yang, B. Liu, H. Li, B. Li, K. Xie, and S. Xie, "Learning based channel allocation and task offloading in temporary uav-assisted vehicular edge computing networks," *IEEE Transactions on Vehicular Technology*, vol. 71, no. 9, pp. 9884–9895, 2022.
- [25] M. Khabbaz, J. Antoun, and C. Assi, "Modeling and performance analysis of uav-assisted vehicular networks," *IEEE Transactions on Vehicular Technology*, vol. 68, no. 9, pp. 8384–8396, 2019.
- [26] K. Liu and J. Zheng, "Uav trajectory planning with interference awareness in uav-enabled time-constrained data collection systems," *IEEE Transactions on Vehicular Technology*, vol. 73, no. 2, pp. 2799–2815, 2024.
- [27] K. Deb, A. Pratap, S. Agarwal, and T. Meyarivan, "A fast and elitist multiobjective genetic algorithm: NSGA-II," *IEEE Transactions on Evolutionary Computation*, vol. 6, no. 2, pp. 182–197, 2002.
- [28] X. Zhu, L. Zhai, N. Li, Y. Li, and F. Yang, "Multi-objective deployment optimization of uavs for energy-efficient wireless coverage," *IEEE Transactions on Communications*, vol. 72, no. 6, pp. 3587–3601, 2024.
- [29] J. Li, Y. Niu, H. Wu, B. Ai, R. He, N. Wang, and S. Chen, "Joint optimization of relay selection and transmission scheduling for uav-aided mmwave vehicular networks," *IEEE Transactions on Vehicular Technology*, vol. 72, no. 5, pp. 6322–6334, 2023.
- [30] D. Jang, H. Song, Y. Ko, and H. J. Kim, "Distributed beam tracking for vehicular communications via uav-assisted cellular network," *IEEE Transactions on Vehicular Technology*, vol. 72, no. 1, pp. 589–600, 2023.
- [31] W. Qi, Q. Song, L. Guo, and A. Jamalipour, "Energy-efficient resource allocation for uav-assisted vehicular networks with spectrum sharing," *IEEE Transactions on Vehicular Technology*, vol. 71, no. 7, pp. 7691–7702, 2022.
- [32] L. Spampinato, D. Ferretti, C. Buratti, and R. Marini, "Joint trajectory design and radio resource management for uav-aided vehicular networks," *IEEE Transactions on Vehicular Technology*, vol. 74, no. 1, pp. 847–860, 2025.
- [33] Q. Zhu, R. Liu, Z. Wang, Q. Liu, and C. Chen, "Sensing-communication co-design for uav swarm-assisted vehicular network in perspective of doppler," *IEEE Transactions on Vehicular Technology*, vol. 73, no. 2, pp. 2578–2592, 2024.
- [34] M. Andrychowicz, M. Denil, S. Gomez, M. W. Hoffman, D. Pfau, T. Schaul, B. Shillingford, and N. de Freitas, "Learning to learn by gradient descent by gradient descent," in *Advances in Neural Information Processing Systems*, 2016.
- [35] M. Zaheer, S. Kottur, S. Ravanbakhsh, B. P. 'oczos, R. Salakhutdinov, and A. Smola, "Deep sets," in *Advances in Neural Information Processing Systems*, 2017.
- [36] J. Lee, Y. Lee, J. Kim, A. Kosiorek, S. Choi, and Y. W. Teh, "Set transformer: A framework for attention-based permutation-invariant neural networks," in *Proceedings of the 36th International Conference on Machine Learning*, 2019, pp. 3744–3753.
- [37] H. Zhao, L. Jiang, J. Jia, P. H. S. Torr, and V. Koltun, "Point transformer," in *Proceedings of the IEEE/CVF International Conference on Computer Vision*, 2021, pp. 16 259–16 268.
- [38] A. Vaswani, N. Shazeer, N. Parmar, J. Uszkoreit, L. Jones, A. N. Gomez, L. Kaiser, and I. Polosukhin, "Attention is all you need," in *Advances in Neural Information Processing Systems*, 2017.
- [39] A. Jaegle, F. Gimeno, A. Brock, O. Vinyals, A. Zisserman, and J. Carreira, "Perceiver io: A general architecture for structured inputs and outputs," in *Proceedings of the 38th International Conference on Machine Learning*, 2021.
- [40] R. Krajewski, J. Bock, L. Kloeker, and L. Eckstein, "The highd dataset: A drone dataset of naturalistic vehicle trajectories on german highways for validation of highly automated driving systems," in *2018 21st International Conference on Intelligent Transportation Systems (ITSC)*, 2018, pp. 2118–2125.